Dalton Transactions

Accepted Manuscript

ROYAL SOCIETY OF CHEMISTRY

www.rsc.org/dalton

Special Issue: **Synergy between Experiment and Theory** 1

Six-Coordinate High-Spin Iron(II) Complexes with Bidentate PN Ligands based on 2-Aminopyridine – New Fe(II) Spin Crossover Systems†

Christian Holzhacker,[a] Maria José Calhorda,[b] Adrié Gil,[b] Maria Deus Carvalho,[b] Liliana P. Ferreira,[c,d] Berthold Stöger,[e] Kurt Mereiter,[e] Matthias Weil,[e] Danny Müller,[a] Peter Weinberger,[a] Ernst Pittenauer,[e] Günter Allmaier,[e] and Karl Kirchner* [a]

Abstract. Several new octahedral iron(II) complexes of the type $[Fe(PN^{R}\text{-}Ph)_2X_2]$ (X = Cl, Br; R = H, Me) containing bidentate PN^{R}-Ph (R = H, Me) (**1a**,**b**) ligands based on 2-aminopyridine were prepared. ^{57}Fe Mössbauer spectroscopy and magnetization studies confirmed in all cases their high spin nature at room temperature with magnetic moments very close to 4.9 μ_B reflecting the expected four unpaired d-electrons in all these compounds. While in the case of the PN^{H}-Ph ligand an S = 2 to S = 0 spin crossover was observed at low temperatures, complexes with the N-methylated analog PN^{Me}-Ph retain an S = 2 spin state also at low temperatures. Thus, $[Fe(PN^{H}\text{-}Ph)_2X_2]$ (**2a**,**3a**) and $[Fe(PN^{Me}\text{-}Ph)_2X_2]$ (**2b**,**3b**) adopt different geometries. In the first case a *cis-Cl,P,N*-arrangement seems to be most likely, as supported by various experimental data derived from ^{57}Fe Mössbauer spectroscopy, SQUID magnetometry, UV/Vis, Raman, and ESI-MS as well as DFT and TDDFT calculations, while in the case of the PN^{Me}-Ph ligand a *trans-Cl,P,N*-configuration is adopted. The latter is also confirmed by X-ray crystallography. In contrast to $[Fe(PN^{Me}\text{-}Ph)_2X_2]$ (**2b**,**3b**), $[Fe(PN^{H}\text{-}Ph)_2X_2]$ (**2a**,**3a**) is labile and undergoes rearrangement reactions. In CH_3OH, the diamagnetic dicationic complex $[Fe(PN^{H}\text{-}Ph)_3]^{2+}$ (**5**) is formed *via* the intermediacy of *cis-P,N*-$[Fe(\kappa^2\text{-}P,N\text{-}PN^{H}\text{-}Ph)_2(\kappa^1\text{-}P\text{-}PN^{H}\text{-}Ph)(X)]^{+}$ (**4a**,**b**) where one PN ligand is coordinated in κ^1-*P*-fashion. In CH_3CN the diamagnetic dicationic complex *cis-N,P,N*-$[Fe(PN^{H}\text{-}Ph)_2(CH_3CN)_2]^{2+}$ (**6**) is formed as major isomer where the two halide ligands are replaced by CH_3CN.

[a] Institute of Applied Synthetic Chemistry, Vienna University of Technology, Getreidemarkt 9, A-1060 Vienna, AUSTRIA, e-mail: kkirch@mail.tuwien.ac.at

[b] Centro de Química e Bioquímica/DQB, Faculdade de Ciências, Universidade de Lisboa, 1749-016 Lisboa, PORTUGAL

[c] Centro de Física da Matéria Condensada/DF, Faculdade de Ciências, Universidade de Lisboa, 1749-016 Lisboa, PORTUGAL,

[d] Departamento Física, Faculdade Ciências e Tecnologia, Universidade de Coimbra, 3004-516 Coimbra, PORTUGAL

[e] Institute of Chemical Technologies and Analytics, Vienna University of Technology, Getreidemarkt 9, A-1060 Vienna, AUSTRIA

†Electronic supplementary information (ESI) available. Atomic coordinates and energies for all optimized species. Calculated and experimental UV/Vis, FIR and Raman spectra of **2a**. CCDC 981196 - 981198 for **2b**, **5**, and **6**. For ESI and crystallographic data in CIF or other electronic format see DOI: xxxxxxx.

Introduction

Heterodifunctional ligands are intensively studied and applied in coordination and organometallic chemistry owing to the often unique properties of their metal complexes and their ability to generate hemilabile systems which often display enhanced reactivity.[1] In particular soft/hard, e.g., P/N assemblies are able to coordinate reversibly to a metal center providing or protecting temporarily a vacant coordination site, a feature very desirable for catalysts. In this context, we have become interested in heterodifunctional PN ligands based on 2-aminopyridine in which the aromatic pyridine ring is separated from the phosphine moiety by an amino group. These types of ligands are easily constructed by reacting 2-aminopyridines with R_2PCl (R = alkyl, aryl) in the presence of base.[2] Owing to the relative ease of phosphorus-nitrogen bond forming reactions compared to those involving phosphorus-carbon bonds, it is not surprising that the synthesis and reactivity of many examples of transition metal complexes featuring this type of PN ligands have been reported over the last decades.[3,4,5,6,7,8,9,10,11,12,13,14] The most prominent member of this ligand family, with a few exceptions,[15] is *N*-diphenylphosphino-2-aminopyridine (PN^H-Ph). Examples of iron complexes containing the PN^H-Ph ligand are very scarce.[16]

Scheme 1

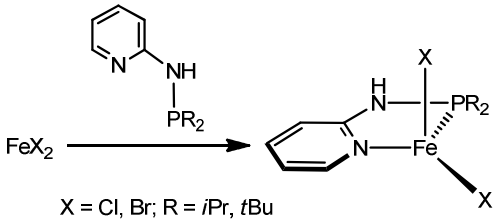

As iron complexes are concerned we have recently shown[3a] that anhydrous FeX_2 (X = Cl, Br) reacts with the bulky and strongly electron donating PN ligands *N*-diisopropylphosphino-2-aminopyridine (PN^H-*i*Pr) and N-di-*tert*-butylphosphino-2-aminopyridine (PN^H-*t*Bu) to form stable coordinatively unsaturated 14e iron(II) complexes of the types $[Fe(PN^H\text{-}R)X_2]$ (Scheme 1). The formation of these complexes is independent of whether 1 or 2 equivs of ligand are used. Interestingly, despite of being highly unsaturated, these complexes turned out to be inert towards the addition of CO.

Here we report the reactions of anhydrous FeX_2 with the ligands PN^H-Ph and PN^{Me}-Ph (Scheme 2) which are sterically less demanding as well as less electron donating than their *i*Pr and *t*Bu congeners. These modifications result in the synthesis of octahedral high spin complexes of the general formula $[Fe(PN^R\text{-}Ph)_2X_2]$. Surprisingly, the additional modification of the ligand scaffold by introducing a methyl group instead of H leads to the formation of isomers with strikingly different chemical properties. In fact, $[Fe(PN^H\text{-}Ph)_2X_2]$ is substitutionally labile in solution and exhibits a high spin/low spin crossover in the solid state, contrasting with the behavior of $[Fe(PN^{Me}\text{-}Ph)_2X_2]$. Notably, octahedral Fe(II) spin crossover complexes with phosphine ligands which are able to switch between

the low-spin and high-spin states are rare.[17] This work is aimed at exploring and understanding the structural and electronic properties of [Fe(PN^R-Ph)$_2X_2$] complexes by means of various experimental data derived from ^{57}Fe Mössbauer spectroscopy, SQUID magnetometry, UV/Vis, Raman, and ESI-MS in synergy with theoretical calculations utilizing DFT and TDDFT methods.

Scheme 2

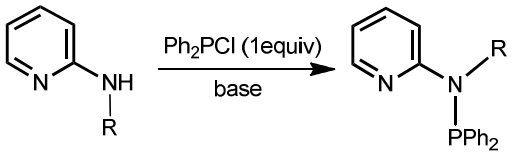

PN^R Ligands

R = H (**1a**), Me (**1b**)

Results and discussion

In sharp contrast to reactions with the bulky ligands PN^H-*i*Pr and PN^H-*t*Bu (Scheme 1), treatment of anhydrous $FeCl_2$ with 2 equiv of the PN ligands PN^H-Ph (**1a**) and PN^{Me}-Ph (**1b**) in THF at room temperature for 12h afforded pale yellow octahedral complexes of the general formula [Fe(PN^R-Ph)$_2Cl_2$] (**2a,b**) in 85 and 92% isolated yields (Scheme 3). The analogous bromide complexes [Fe(PN^R-Ph)$_2Br_2$] (**3a**,**b**) were obtained in similar fashion by straightforward complexation of the respective free PN ligands with anhydrous ferrous dibromide in 83 to 91% yields. The formation of these complexes is independent of whether 1 or 2 equivs of ligand are used. However, in the first case substantial amounts of FeX_2 remained

Scheme 3

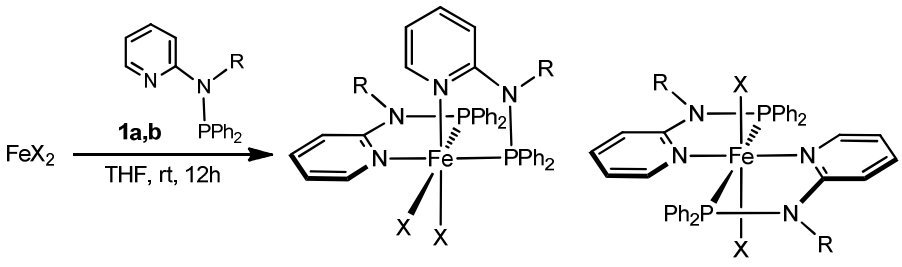

2a R = H; X = Cl
3a R = H; X = Br

2b R = Me, X = Cl
3b R = Me, X = Br

unreacted. There was no evidence for the formation of tetra-coordinate [Fe(PN^R-Ph)X_2] as in the case of the more electron donating and bulkier PN^H-*i*Pr and PN^H-*t*Bu ligands (Scheme 2). In the solid state all complexes are thermally stable if air is excluded. In solution **2a** and **3a** turned out to be highly unstable forming different decomposition products depending on the solvent (*vide infra*). On the other

hand, **2b** and **3b** are stable in most common solvents such as CH_3OH, THF, CH_2Cl_2, and CH_3CN for several days without showing any noticeable decomposition. In fact, even single crystals suitable for X-ray diffraction measurements could be grown for **2b**. This behavior clearly suggests that **2a** and **3a** are structurally different from **2b** and **3b**. It has to be kept in mind that for complexes of the general formula $[Fe(PN^R\text{-}Ph)_2X_2]$ in principle five different coordination isomers are conceivable as illustrated in Scheme 4.

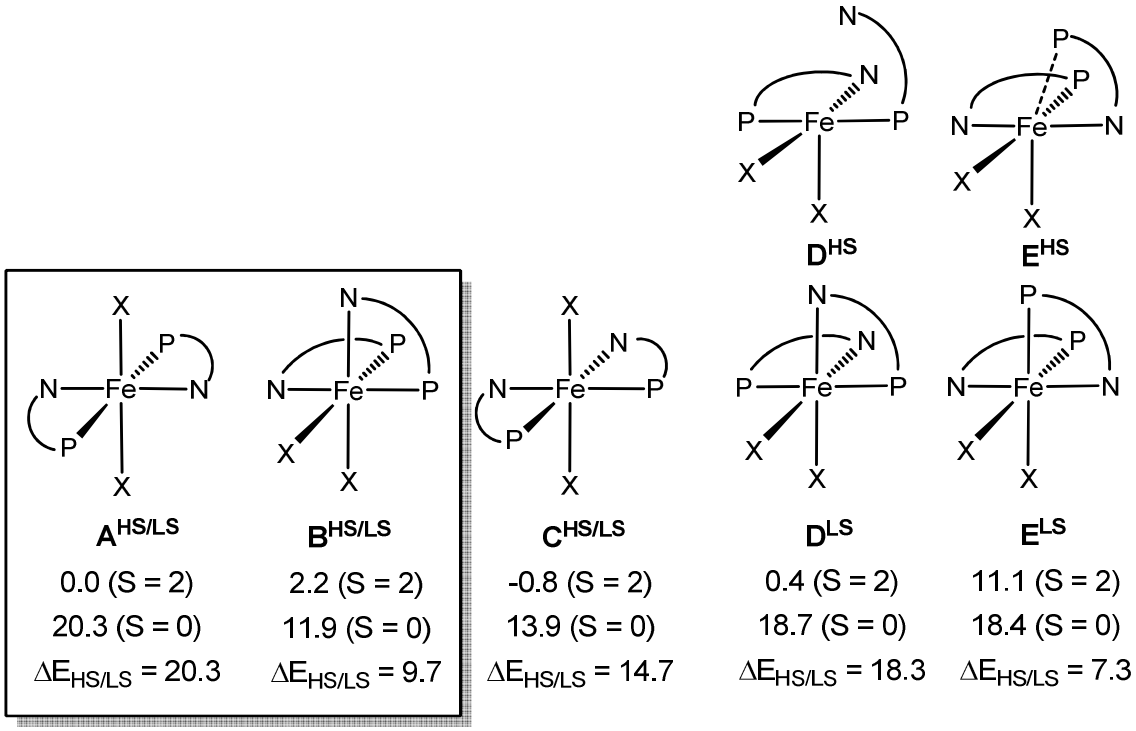

Scheme 4 (DFT calculated geometries and electronic energies in kcal/mol for X = Cl and PN = PN^H-Ph)

The molecular structure of **2b**, depicted in Figure 1, reveals that all Cl, P and N atoms are in *trans* position to one another. Accordingly, in the case of complexes bearing the PN^{Me}-Ph (**1b**) ligand isomer **A** in its high spin form is the thermodynamically most stable species. This finding is also supported by DFT calculations (*vide infra*).

Figure 1

In order to establish the nature of the isomer formed in the case of complexes **2a** and **3a** featuring the PN^H-Ph ligand (**1a**), reactivity studies in different solvents were carried out. Additionally, a variety of measurements including SQUID magnetometry, ^{57}Fe Mössbauer spectroscopy, UV/Vis, Raman, ESI-MS as well as DFT calculations were performed. Due to the instability of **2a** and **3a** in solution as well as the paramagnetic nature of complexes **2a**,**b** and **3a**,**b**, bearing basically aromatic

protons and carbon atoms, ^{1}H NMR spectra exhibited only very broad and featureless signals and were thus not very informative. $^{13}C\{^{1}H\}$ and $^{31}P\{^{1}H\}$ NMR signals could not be detected at all.

In CH_3OH complexes **2a** and **3a** are substitutionally labile and undergo rearrangement reactions to yield the diamagnetic dicationic *tris*-PN^H-Ph complex $[Fe(PN^H\text{-}Ph)_3]^{2+}$ (**5**) (Scheme 5, reaction is not balanced) together with free ligand PN^H-Ph, the paramagnetic tetrahaloferrate anion FeX_4^{2-} and intractable paramagnetic materials. Monitoring of this reaction by $^{31}P\{^{1}H\}$ NMR spectroscopy revealed that this reaction proceeds *via* the intermediates *cis-P,N*-$[Fe(\kappa^2\text{-}P,N\text{-}PN^H\text{-}Ph)_2(\kappa^1\text{-}P\text{-}PN^H\text{-}Ph)(X)]^+$ (**4a,b**) where one PN ligand is coordinated in κ^1-*P*-fashion. This reaction involves an intermolecular ligand transfer between two $[Fe(PN^H\text{-}Ph)_2X_2]$ complexes and is complete within about 15 minutes at room temperature. In the $^{31}P\{^{1}H\}$ NMR spectrum (measured at a 600 MHz NMR spectrometer), intermediate **4a** displays an ABX pattern providing further evidence for a *cis-Cl,P,N*-structure (isomer **B**) of the starting materials **2a** and **3a** (Scheme 4). Intermediate **4b** still exhibits a simpler A_2X spin system ($\delta_A \approx \delta_B$). The rational synthesis of **5** (as chloride **5a** or bromide salt **5b**) can be achieved in 90 and 94% isolated yield by reacting anhydrous FeX_2 with 3 equivs. of PN^H-Ph in CH_3OH.

Scheme 5

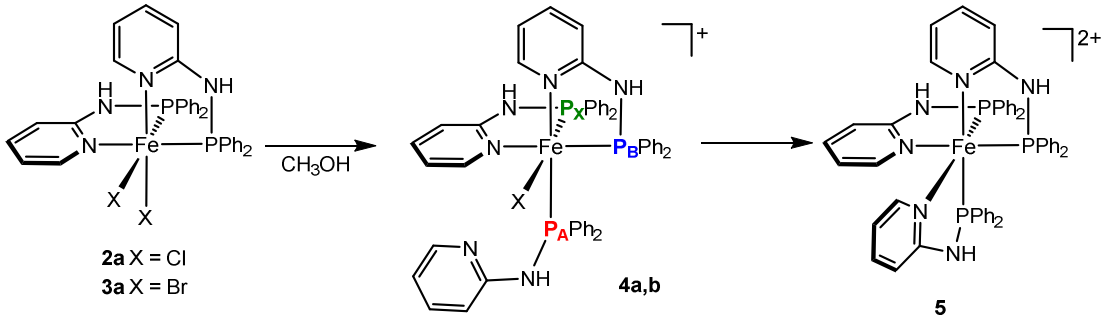

This complex gives rise to a singlet in the $^{31}P\{^{1}H\}$ NMR spectrum at 104.5 ppm indicating that all P and N atoms, respectively, are *cis* to one another. The structure of **5** (as bromide salt) was unequivocally established by X-ray crystallography. A structural view is depicted in Figure 2 with selected bond distances given in the caption.

Scheme 6

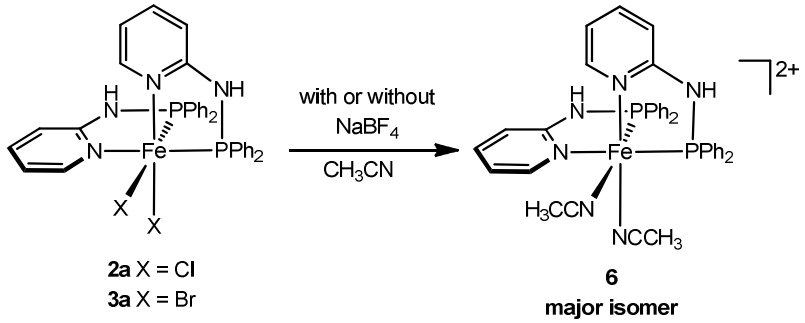

Upon dissolution of **2a** and **3a** in acetonitrile a mixture of the diamagnetic dicationic complex *cis-N,P,N*-$[Fe(PN^H\text{-}Ph)_2(CH_3CN)_2]^{2+}$ (**6**) and an unidentified complex, presumably a symmetrical isomer of **6**, in a 2:1 molar ratio was afforded within 24h. Complex **6** displays an AB pattern for the two nonequivalent ^{31}P nuclei centered at 114.6 ppm ($\Delta\nu$ = 533.2 Hz) with a coupling constant J_{PP} of 54.8 Hz. The small coupling constant is consistent with a *cis*-P,P arrangement. The minor isomer gives rise to a singlet at 110.8 ppm (for complexes of the formula $[Fe(PN^H\text{-}Ph)_2(CH_3CN)_2]^{2+}$ four isomers are conceivable which would all give rise to a singlet in the $^{31}P\{^1H\}$ NMR spectrum, *cf* isomers **A**, **C**, **D**, and **E** in Scheme 4).

Figure 2

It has to be noted, that in the presence of $NaBF_4$ as halide scavenger the same complexes were formed in about the same molar ratio. From this mixture crystals of **6** suitable for an X-ray diffraction study were obtained. A molecular view of **6** is depicted in Figure 3 with selected bond distances given in the caption. The dicationic iron complex adopts a slightly distorted octahedral geometry around the metal center with all donor atoms of the CH_3CN and PN^H-Ph ligands being in *cis* position to one another. If the formation of **6** is the result of two consecutive dissociative substitution processes, the starting materials **2a** and **3a** most likely adopt the all *cis* form $\mathbf{B^{HS}}$ as in this case no further rearrangement steps are required.

Figure 3

Upon cooling to 77 K the color of complexes **2a** and **3a** changed from pale yellow to dark violet suggesting possible high-spin/low-spin transitions. In agreement with this observation, the UV/Vis spectrum of **2a** and **3a** in the solid state at 293 K did not shown any absorption in the visible range, while at 123 K these complexes exhibited two bands at 562 and 690 nm and 565 and 716 nm, respectively. On the other hand, all other complexes did not change their color at low temperature again suggesting that the structures of **2a** and **3a** are significantly different from those of **2b** and **3b**.

The magnetic properties of all compounds were studied by SQUID magnetometry and ^{57}Fe Mössbauer spectroscopy. The temperature dependent magnetic behavior of complexes **2a** and **3a** (Figure 4), in agreement with the color changes, shows that both compounds exhibit a thermal and almost complete spin transition (ST) with $\chi_m T$ values near 3.0 $cm^3\,mol^{-1}\,K$ at 300 K consistent with HS Fe(II), and $\chi_m T$ values below 0.4 $cm^3\,mol^{-1}\,K$ at 10 K, corresponding to a high fraction of LS Fe(II) and a residual content of HS Fe(II), as confirmed by Mössbauer spectra. Both samples were measured on cooling and warming sequences displaying gradual spin transitions without thermal hysteresis, maintaining the low temperature LS Fe(II) fraction up to approximately 125 K (**2a**) or 150 K (**3a**). At those temperatures the population of the HS state gradually increases, achieving full conversion over a temperature range of 125 K (**2a**) or 150 K (**3a**). The ST temperatures, $T_{1/2}$, can be assumed as 185 K for **2a** and 222 K for **3a** (Figure 4, inset). These first-order spin transitions, somewhat gradual, not complete at low temperatures and displaying no thermal hysteresis, are more likely to be associated to

weak intermolecular cooperative effects, without structural phase transitions.[18,19] Although hydrogen-bonded networks can induce cooperative interactions, and their existence cannot be discarded in the presence of the PN^{H}-Ph ligand, they should be relatively weak since the complexes are neutral and there is no charge assistance.[19]

Figures 4 and **5**

^{57}Fe Mössbauer results are in good agreement with magnetization data, as can be seen from Figure 5 and Table 1. At room temperature only one quadrupole doublet characteristic of HS Fe(II) with isomer shift values (δ) of 0.87(1) mm s^{-1} and quadrupole splitting values (ΔE_Q) around 3.1(1) mm s^{-1} are detected for both complexes **2a** and **3a**. A second quadrupole doublet attributed to LS Fe(II) appears and its fraction increases as the temperature decreases. At 78 K the hyperfine parameters δ = 0.48(1) mm s^{-1} and $\Delta E_Q \approx$ 1.0(1) mm s^{-1} confirm the LS state of Fe(II) with relative fractions of 87% for the Cl

Figures 6 and **7**

compound and 92% for the Br one, assuming the same Debye-Waller factor for LS and HS species. According to the magnetization data, the HS fraction existing at this temperature should remain until 10 K.

The thermal variation of the inverse molar magnetic susceptibility and of $\chi_m T$ for complexes **2b** and **3b** is shown in Figure 6. Upon replacement of the NH moiety by a NMe unit the spin transition completely vanishes, indicating an increased energy difference between the HS and LS forms in the 2b and 3b complexes when compared with 2a and 3a ones. The thermal variation of χ_m^{-1} is well described by a modified Curie law ($\chi_m = C_m/T+K$, where C_m is the molar Curie constant and K is a temperature independent constant). Iron effective magnetic moments of 5.0(1) and 5.1(1) μ_B were extracted from the C_m values of the Cl and Br complexes, respectively, in good agreement with the effective magnetic moment of HS Fe(II) in the spin-only approximation (4.9 μ_B).

^{57}Fe Mössbauer spectra collected at room temperature for **2b** and **3b** also agree with magnetization data since only one iron site (one quadrupole doublet) with hyperfine parameters characteristics of HS Fe(II) is observed: δ = 0.85(1) and 0.88(1) mm/s and ΔE_Q = 3.04(1) and 3.14(1) mm/s for the Cl and Br complexes, respectively (Figure 7, Table 2). Comparing room temperature hyperfine parameters obtained for all octahedral compounds, it is clear that the substitution of the NH moiety by a NMe unit does neither change significantly the s-electron density at the iron nuclei (related with δ) nor the quadrupole splitting values. This latter parameter depends on the electric field gradient (EFG) surrounding the Fe nuclei with two contributing sources: the lattice (charges in a non-cubic symmetry) surrounding the Mössbauer probe and the iron valence electrons. As similar values were obtained for *trans* and *cis* complexes and rather different values were obtained for the *cis* compound

in high and low spin states, it can be deduced that the main contribution for the EFG comes from the iron valence electrons.

The ^{57}Fe Mössbauer parameters were calculated for the isomer **B** (see below) of complex **2a** with a DFT approach (using ORCA[20] and two basis sets, b1 and b2; see Experimental details). The electronic density at the nucleus (ρ) was converted in isomer shifts (δ), using the method of Neese[21] and the quadrupole splitting was obtained directly. The isomer shifts are 0.835 (HS) and 0.611 (LS) mm/s with the b1 basis, and 0.736 and 0. 515 mm/s, respectively with the better b2 basis set. The quadrupole splittings were calculated as 0.579, 3.009 (b1) and 0.579, 3.026 (b2) mm/s, for LS and HS, respectively. Both are good estimates of the experimental parameters. The same calculation (b1) for isomer **C** led to similar isomer shifts (0.830 and 0.631 mm/s, for HS and LS), and quadrupole splitting for the LS isomer (0.620 mm/s). However, the quadrupole splitting for the HS room temperature species is calculated as 2.398 mm/s, very far from the experimental value. This suggests that isomer **B** is the most likely species to be present in the solid.

Moreover, all complexes were also investigated by means of ESI-MS (Table 3). Solutions of complexes **2a**, **2b**, **3a,** and **3b** in CH_3OH in the presence of NaX (X = Cl, Br) were subjected to ESI-MS analysis in the positive ion mode. By means of the so called "soft ionization" technique ESI at atmospheric pressure, the most abundant signals are observed at m/z is 647.10, 675.13, 691.05, and 719.08, respectively, which correspond to the cationic complexes $[Fe(PN^R\text{-}Ph)_2X]^+$ ($[M-X]^+$), where one halide ligand is dissociated. Further abundant fragments are $[M\text{-}X\text{-}HX]^+$ (only for **2a** and **3a**), [M-X-**1a**]$^+$, and [M-X-**1b**]$^+$. Representative corresponding positive ion ESI full scan mass and MS/MS (low energy CID) spectra of **3a** are depicted in Figure 8. Furthermore in the inset of Figure 8 (A) the isotopic pattern of $[M-Br]^+$ ion is compared with the theoretical pattern, which turned out to correlate quite well.

Figure 8

The geometries and energies (in kcal/mol) of all possible isomers of **2a** and **3a** in two different spin states (S = 2 and S = 0) were determined by means of DFT/OPBE calculations (Scheme 4, electronic energies shown for all isomers of **2a**). Isomer $\mathbf{A}^{HS}$ was used as reference point for all calculations. Stable minima in both S = 2 and S = 0 spin states could be obtained for all five isomers.

In all cases the quintet ground state (S = 2) is thermodynamically more stable and the energies of isomers $\mathbf{A}^{HS}$-$\mathbf{D}^{HS}$ are very similar ranging from -0.8 to 2.2 kcal/mol, while $\mathbf{E}^{HS}$ is less stable than $\mathbf{A}^{HS}$ by 11.1 kcal/mol. All of these four isomers are possible high spin species. It is interesting to note, however, that isomers $\mathbf{D}^{HS}$ and $\mathbf{E}^{HS}$ are structurally significantly different from the other isomers. These complexes are five coordinate species adopting a distorted square pyramidal geometry. While in $\mathbf{D}^{HS}$ one pyridine moiety is no longer coordinated to the iron center (the Fe···N_{py} distance is 3.86 Å), in $\mathbf{E}^{HS}$ one phosphine moiety is weakly bound with a Fe-P bond distance of 3.10 Å. In fact, isomer $\mathbf{D}^{HS}$ strongly resembles five coordinate PNP pincer complexes of the type $[Fe(PNP)Cl_2]$ which form stable HS complexes with a quintet ground state that show no spin crossover.[22] The corresponding singlet ground states $\mathbf{A}^{LS}$-$\mathbf{E}^{LS}$, all with an octahedral geometry, are less stable than the corresponding HS

states. The energy differences between HS and LS spin states ($\Delta E_{HS/LS}$) of isomers **A**-**E** are 20.3, 9.7, 14.7, 18.3, and 7.3 kcal/mol. It is, thus, reasonable that at low temperatures no spin-crossover takes place in the case of isomer **A**, which displays a very high energy difference. Accordingly, a HS/LS crossover is more likely to take place in the case of **B** and to a lesser extent of **C** where (i) the HS species has low energy and (ii) $\Delta E_{HS/LS}$ is small. In contrast, spin transitions in **D** and **E** would be associated with severe structural changes, e.g., changes of both geometry and coordination number (Scheme 4), which appear to be unlikely to occur in the solid state and are not suggested by any experimental data. The high-spin state exhibits typically longer metal ligand bonds, since the partially occupied e_g* states are metal-ligand anti-bonding. In the present case of the $[Fe(PN^R\text{-}Ph)_2X_2]$ complexes this effect is very pronounced for the Fe-P and Fe-N bonds (for instance, Fe-N1 shortens from 2.388 to 1.967 Å, and Fe-P1 from 2.529 to 2.151 Å) but modest for the Fe-Cl bonds (Table 4). There are several literature examples of octahedral Fe(II) diphosphine complexes of the types $[Fe(PP)_2X_2]$ (PP = *cis*-1,2-bis(diphenylphosphino)ethylene, X = Cl, Br) where the Fe-P bonds are abnormally long in the quintet ground state.[17] Based on these calculations, we propose that **2a** and **3a** adopt a *cis-Cl,P,N*-geometry (**B**). The structures of the HS and LS isomers of **B** are shown in Figure 9. However, a *cis-P,N-trans-Cl* arrangement (**C**) cannot be conclusively ruled out.

Figure 9

As was shown above, the Mössbauer parameters calculated for isomer **B** of complex **2a** are in good agreement with those determined experimentally for the HS and the LS species, contrary to isomer **C**. Since there is a pronounced color change from pale yellow to dark violet, we also calculated the electronic spectrum of the two spin states of isomers **B** and **C** of complex **2a**. The high spin forms exhibit very weak absorptions in the visible, with the bands at 392.7 nm (**B**) or 368.7 nm (**C**) representing the beginning of the UV strong absorptions, and both are consistent with the pale color of the complex. On the other hand, the spectra of the low spin forms are dominated by the strong absorptions at 545.5 nm (**B**) or 559.8 nm (**C**), with another weaker one (684.5 nm) for **B** and two weaker ones (647.0 and 709.1 nm) for **C**. The agreement between calculated and experimental spectra (562 and 690 nm) is slightly better for isomer **B** reinforcing the idea that it corresponds to the observed isomer of **2a.**

To get further evidence for the above suggested *cis*-configuration, vibrational spectroscopy (FIR, Raman) was performed. While the Raman spectra did not reveal characteristic vibrations allowing a distinction between the different isomers, in the FIR characteristic bands associated with Fe-Cl and Cl-Fe-Cl vibrations could be identified. In the theoretically obtained FIR of the *cis*-isomer $\mathbf{B}^{HS}$ two characteristic Fe-Cl stretching vibrations are found at 252 and 276 cm^{-1}, whereas for the *trans*-isomer $\mathbf{C}^{HS}$ vibrations at 141 and 298 cm^{-1} are observed which are assignable to the Cl-Fe-Cl bending mode and the asymmetric Cl-Fe-Cl stretching frequency, respectively. In the experimentally obtained spectrum, despite of the weak signals, the two expected bands for the *cis*-product are observed at 253 and 278 cm^{-1}, while the characteristic asymmetric Cl-Fe-Cl stretching mode expected for $\mathbf{C}^{HS}$ (and $\mathbf{A}^{HS}$) is missing. Thus, the experimental FIR data seem to support the *cis*-configuration,

as the respective spectral features in the two *trans* isomers are missing. One has to keep in mind however that the experimental IR and Raman spectra are obtained for bulk solid samples, while the calculated spectra correspond to single isolated molecules in the gas-phase.

Conclusion

In the present work we have prepared stable octahedral 18e iron(II) complexes of the general formula $[Fe(PN^{R}\text{-}Ph)_2X_2]$ (R = H, Me) by reacting anhydrous FeX_2 with 2 equivs of PN^{R}-Ph ligands. Tetrahedral complexes of the type $[Fe(PN^{R}\text{-}Ph)X_2]$ as in the case of the bulkier PN-*i*Pr and PN-*t*Bu ligands were not formed. ^{57}Fe Mössbauer spectroscopy and magnetization studies confirmed their high spin nature with magnetic moments very close to 4.9 μ_B at room temperature reflecting the expected four unpaired d-electrons in all these compounds. While in the case of the PN^{H}-Ph ligand a S = 2 to S = 0 spin crossover was observed at low temperatures, complexes with the N-methylated analog PN^{Me}-Ph maintain the high spin state also at low temperatures. It should be emphasized that this is the first example of spin crossover in this type of complexes with heterodifunctional PN ligands. Accordingly, complexes $[Fe(PN^{H}\text{-}Ph)_2X_2]$ and $[Fe(PN^{Me}\text{-}Ph)_2X_2]$ adopt different coordination geometries. For complexes of the general formula $[Fe(PN^{R}\text{-}Ph)_2X_2]$ in principle five different coordination isomers are conceivable. While in $[Fe(PN^{Me}\text{-}Ph)X_2]$ all donor atoms of the two PN^{Me}-Ph ligands are *trans* to one another, i.e., a *trans-Cl,P,N*-geometry is adopted, in $[Fe(PN^{H}\text{-}Ph)X_2]$ the PN ligands most likely exhibit a *cis-Cl,P,N*-arrangement. The structural assignments are based on reactivity studies and various experimental data derived from ^{57}Fe Mössbauer spectroscopy, SQUID magnetometry, UV/Vis, Raman, and ESI-MS as well as theoretical considerations by means of DFT and TDDFT calculations. In the case of $[Fe(PN^{Me}\text{-}Ph)Cl_2]$ the geometry is unequivocally established by X-ray crystallography. Moreover, in contrast to $[Fe(PN^{Me}\text{-}Ph)_2X_2]$, $[Fe(PN^{H}\text{-}Ph)_2X_2]$ is very labile and undergoes rearrangement reactions. In CH_3OH the diamagnetic dicationic complex $[Fe(PN^{H}\text{-}Ph)_3]^{2+}$ is formed *via* the intermediacy of *cis-P,N*-$[Fe(\kappa^2\text{-}P,N\text{-}PN^{H}\text{-}Ph)_2(\kappa^1\text{-}P\text{-}PN^{H}\text{-}Ph)(X)]^{+}$ where one PN ligand is coordinated in κ^1-*P*-fashion. This reaction involves an intermolecular ligand transfer. In CH_3CN the diamagnetic dicationic complex *cis-N,P,N*-$[Fe(PN^{H}\text{-}Ph)_2(CH_3CN)_2]^{2+}$ is formed as major isomer where the two halide ligands are replaced by CH_3CN. In sum, this dual theoretical/experimental approach provides a consistent picture of the chemistry of complexes $[Fe(PN^{H}\text{-}Ph)_2X_2]$ and$[Fe(PN^{Me}\text{-}Ph)_2X_2]$ with respect to their geometries and electronic properties.

Experimental section

General considerations

All manipulations were performed under an inert atmosphere of argon by using Schlenk techniques. The solvents were purified according to standard procedures.[23] The deuterated solvents were purchased from Aldrich and dried over 4 Å molecular sieves. The ligand *N*-diphenylphosphino-2-aminopyridine (PN^{H}-Ph) (**1a**)[24] was prepared according to the literature. ^{1}H, ^{13}C{^{1}H}, and ^{31}P{^{1}H} NMR spectra were recorded on Bruker AVANCE-250, AVANCE-400, and AVANCE DRX 600

spectrometers. ^{1}H and $^{13}C\{^{1}H\}$ NMR spectra were referenced internally to residual protio-solvent, and solvent resonances, respectively, and are reported relative to tetramethylsilane (δ = 0 ppm). $^{31}P\{^{1}H\}$ NMR spectra were referenced externally to H_3PO_4 (85%) (δ = 0 ppm).

Magnetization measurements as a function of temperature were performed on powder samples using a SQUID magnetometer (Quantum Design MPMS). The curves were obtained under 0.1 T, for temperatures ranging from 10 to 300 K, using cooling and warming sequences with a temperature variation rate of 1 K per minute and 1 minute waiting time at each measurement temperature. The molar susceptibility values (χ_m) were corrected for diamagnetism of the constituent atoms using Pascal constants.

The ^{57}Fe Mössbauer spectra were recorded in transmission mode at several temperatures between room temperature and 78 K using a conventional constant-acceleration spectrometer and a 50 mCi ^{57}Co source in a Rh matrix. The low temperature measurements were performed using a liquid nitrogen flow cryostat with a temperature stability of $\pm$0.5 K. The velocity scale was calibrated using an α-Fe foil. The spectra were fitted to Lorentzian lines using the WinNormos software program, and the isomer shifts reported are relative to metallic α-Fe at room temperature.

All mass spectrometric measurements were performed on an Esquire 3000^{plus} 3D-quadrupole ion trap mass spectrometer (Bruker Daltonics, Bremen, Germany) in positive-ion mode electrospray ionization (ESI-MS). Mass calibration was done with a commercial mixture of perfluorinated trialkyl-triazines (ES Tuning Mix, Agilent Technologies, Santa Clara, CA, USA). All analytes were dissolved in methanol “hypergrade for LC-MS Lichrosolv” quality (Merck, Darmstadt, Germany) to a concentration of roughly 1 mg/mL and doped with sodium chloride or sodium bromide (Merck, Darmstadt, Germany) to avoid dissociation of both halogen substituents from the iron cation promoting the corresponding $[M–X]^+$ ion formation (X = Cl, Br) as previously described for molybdenum and titanium complexes[25,26] Direct infusion experiments were carried out using a Cole Parmer model 74900 syringe pump (Cole Parmer Instruments, Vernon Hills, IL, USA) at a flow rate of 2 μl/min. Full scan and MS/MS-scans were measured in the range m/z 100-1100 with the target mass set to m/z 1000. Further experimental conditions include: drying gas temperature: 150°C; capillary voltage: -4 kV; skimmer voltage: 40 V; octapole and lens voltages: according to the target mass set. Helium was used as buffer gas for full scans and as collision gas for MS/MS-scans in the low energy CID (collision induced dissociation) mode. The activation and fragmentation width for tandem mass spectrometric (MS/MS) experiments was set to 6 Da to cover the main isotope cluster for fragmentation. The corresponding fragmentation amplitude ranged from 0.4 to 0.6 V in order to keep a low abundant precursor ion intensity in the resulting MS/MS spectrum. As precursor ions for tandem mass spectrometric experiments the ions $[M-X]^+$ could be selected as precursor ions. All mass calculations are based on the lowest mass (i.e. most abundant) iron isotope (^{56}Fe-isotope). Mass spectra and tandem spectra were averaged during data acquisition time of 1 to 2 min and one analytical scan consisted of five successive micro scans resulting in 50 and 100 analytical scans, respectively, for the final mass spectrum or MS/MS spectrum.

Raman spectra were collected on a Horiba Jobin Yvon Micro-Raman spectrometer (LabRam 800 HR) equipped with an integral Olympus BX 41 microscope (20f objective) and a Peltier-cooled CCD detector, using the 632.8 nm line of a He–Ne laser (1.5 mW) for excitation. A 600 line grating

was used for obtaining the Raman spectrum. The Raman–Stokes spectra were recorded in the 4000–200 cm^{-1} range of Raman shifts at 1.3 cm^{-1} spectral resolution; $\tilde{\nu}$ in cm^{-1}; relative intensities are given in % of the most intense peak. The spectrograph was calibrated using a Si-wafer at 520 cm^{-1} Raman-shift.Far IR spectra were recorded within the range 700 cm^{-1} to 100 cm^{-1} on a Perkin-Elmer 400 FIR FTIR spectrometer, equipped with a PikeTechnologies GladiATR using a diamond crystal plate.

Electronic spectra of the undiluted powder samples have been measured using a Perkin Elmer Lambda 900 UV-VIS-NIR spectrometer equipped with a thermostatable powder sample holder in diffuse reflection geometry (Praying Mantis accessory®) between 335 nm and 1200 nm within the temperature range of 123 K and 298 K.

Syntheses

PN^{Me}-Ph (1b). A solution of *n*-BuLi in *n*-hexane (2.5 M, 16.5 mL, 41.11 mmol) was added slowly to a solution of N-methylpyridine-2-amine (4.23 g, 39.15 mmol) in toluene (150 mL) at -10°C. After stirring at room temperature for 3 h, the red solution was cooled to -30°C, chlorodiphenylphosphine was added and the mixture was stirred at 80°C for 12 h. The LiCl was filtered over pre-dried Celite® and the remaining clear yellow solution was concentrated under vacuum. The product was isolated as a white solid. Yield: 8.89 g (78%). Anal. Calcd. for $C_{18}H_{17}N_2P$ (292.32): C, 73.96; H, 5.86; N, 9.58%. Found: C, 73.85; H, 5.98; N, 9.61%. ^{1}H NMR (δ, CD_2Cl_2, 20°C): 8.21 (d, 1H, *J* = 2.9 Hz, py^6), 7.53 (t, 1H, *J* = 7.7 Hz, py^4), 7.47 - 7.35 (m, 11H, py^3, ph), 6.75 (t, 1H, *J* = 5.5 Hz, py^5), 2.91 (s, 3H, NCH_3). $^{13}C\{^1H\}$ NMR (δ, CD_2Cl_2, 20°C): 161.2 (d, $^2J_{CP}$ = 26.8 Hz, py^2), 147.5 (s, py^6), 136.9 (s, py^4), 136.8 (d, $^1J_{CP}$ = 14.0 Hz, Ph^1), 131.9 (d, $^3J_{CP}$ = 20.9 Hz, $Ph^{3,5}$), 128.9 (s, Ph^4), 128.5 (d, $^2J_{CP}$ = 4.6 Hz, $Ph^{2,6}$), 114.6 (s, py^5), 110.4 (d, $^3J_{CP}$ = 20.9 Hz, py^3), 34.1 (d, $^2J_{CP}$ = 8.25 Hz, NCH_3). $^{31}P\{^1H\}$ NMR (δ, CD_2Cl_2, 20°C): 62.7.

***cis*-*Cl,P,N*-[Fe(PN^H-Ph)$_2$$Cl_2$] (2a).** A solution of anhydrous $FeCl_2$ (111 mg, 0.88 mmol) and PN^H-Ph (**1a**) (500 mg, 1.80 mmol) was stirred in THF (15 mL) at room temperature for 12 h. The solvent was then removed under reduced pressure. The remaining white solid was collected on a glass frit, washed with toluene (15 mL) and twice with diethyl ether (15 mL) and dried at 50°C under vacuum for 3 h. Yield: 510 mg (85%). Anal. Calcd. for $C_{34}H_{30}Cl_2N_4P_2Fe$ (683.34): C, 59.76; H, 4.42; N, 8.20%. Found: C, 59.88; H, 4.48; N, 8.24%. ESI-MS (*m/z,* CH_3OH, NaCl) positive ion: 647.10 $[M-Cl]^+$.

***trans*-*Cl,P,N*-[Fe(PN^{Me}-Ph)$_2$$Cl_2$] (2b).** This complex was prepared analogously to **2a** with anhydrous $FeCl_2$ (100 mg, 0.79 mmol) and PN^{Me}-Ph (**1b**) (473 mg, 1.62 mmol) as starting materials. Yield: 519 mg (92%). Anal. Calcd. for $C_{36}H_{34}Cl_2N_4P_2Fe$ (711.39): C, 60.78; H, 4.82; N, 7.88%. Found: C, 60.65; H, 4.88; N, 7.94%. ESI-MS (*m/z,* CH_3OH, NaCl) positive ion: 675.13 $[M-Cl]^+$.

***cis*-*Cl,P,N*-[Fe(PN^H-Ph)$_2$$Br_2$] (3a).** This complex was prepared analogously to **2a** with anhydrous $FeBr_2$ (189 mg, 0.88 mmol) and **1a** (500 mg, 1.80 mmol) as starting materials. Yield: 562 mg (83%). Anal. Calcd. for $C_{34}H_{30}Br_2N_4P_2Fe$ (772.24): C, 73.96; H, 5.86; N, 9.58%. Found: C, 73.72; H, 5.91; N, 9.50%. ESI-MS (*m/z,* CH_3OH, NaBr) positive ion: 691.05 $[M-Br]^+$.

***trans*-*Cl,P,N*-[Fe(PN^{Me}-Ph)$_2$$Br_2$] (3b).** This complex was prepared analogously to **2b** with anhydrous $FeBr_2$ (176 mg, 0.81 mmol) and **1b** (488 mg, 1.67 mmol) as starting materials. Yield: 595

mg (91%). Anal. Calcd. for $C_{36}H_{34}Br_2N_4P_2Fe$ (800.29): C, 73.96; H, 5.86; N, 9.58%. Found: C, 73.85; H, 5.79; N, 9.68%. ESI-MS (*m/z,* CH_3OH, NaBr) positive ion: 719.08 $[M-Br]^+$.

***cis-P,N*-[Fe(PN^H-Ph)$_3$]Cl$_2$ (5a).** A solution of anhydrous $FeCl_2$ (44 mg, 0.35 mmol) and PN^H-Ph (**1a**) (300 mg, 1.08 mmol) was stirred in CH_3OH (15 mL) at room temperature for 12 h. The red solution was then filtered and the solvent removed under reduced pressure. The remaining pink solid washed twice with diethyl ether (15 mL) and dried at 50°C under vacuum for 3 h. Yield: 301 mg (90%). Anal. Calcd. for $C_{51}H_{45}Cl_2N_6P_3Fe$ (961.63): C, 63.70; H, 4.72; N, 8.74%. Found: C, 63.82; H, 4.69; N, 8.64%. ^{1}H NMR (δ, CD_3OD, 20°C): 7.64 – 7.55 (m, 6H, py, Ph), 7.36 – 7.23 (m, 15H, ph), 7.16 – 7.11 (m, 9H, py, Ph), 7.05 – 6.97 (bs, 6H, Ph), 6.61 (t, *J* = 6.5 Hz, 3H, py) 6.48 (d, *J* = 5.9 Hz, 3H, py), 4.91 (s, 3H, N*H*). ^{13}C{^{1}H} NMR (δ, CD_3OD, 20°C): 163.9 (dd, $^2J_{CP}$ = 3.9 Hz, $^3J_{CP}$ = 7.6 Hz, py^2), 148.8 (s, py^6), 140.1 (s, py^4), 134.97 (dd, $^1J_{CP}$ = 16.0 Hz, $^3J_{CP}$ = 31.1 Hz, Ph), 133.9 (dd, $^1J_{CP}$ = 14.7 Hz, $^3J_{CP}$ = 27.6 Hz, Ph), 131.58 (s, Ph), 131.28 (d, $^2J_{CP}$ = 7.2 Hz, Ph), 131.3 (d, $^2J_{CP}$ = 7.3 Hz, Ph), 130.0 (s, Ph), 129.2 (d, $^3J_{CP}$ = 19.8 Hz, Ph), 129.2 (d, $^3J_{CP}$ = 19.8 Hz, Ph), 129.1 (d, $^3J_{CP}$ = 19.7 Hz, Ph), 129.1 (d, $^3J_{CP}$ = 19.5 Hz, Ph), 128.2 (d, $^2J_{CP}$ = 6.4 Hz, Ph), 128.2 (d, $^2J_{CP}$ = 6.2 Hz, Ph), 117.9 (s, py^5), 112.2 (s, py^3). ^{31}P{^{1}H} NMR (δ, CD_3OD, 20°C): 104.5. ESI-MS (*m/z,* CH_3OH, NaCl) positive ion: 889.22 $[M-Cl-HCl]^+$.

***cis-P,N*-[Fe(PN^H-Ph)$_3$]Br$_2$ (5b).** This complex was prepared analogously to **5a** with anhydrous $FeBr_2$ (75 mg, 0.35 mmol) and **1b** (300 mg, 1:08 mmol) as starting materials. Yield: 343 mg (94%). Anal. Calcd. for $C_{51}H_{45}Br_2N_6P_3Fe$ (1050.53): C, 58.31; H, 4.32; N, 8.00%. Found: C, 58.12; H, 4.39; N, 8.12%. ESI-MS (*m/z,* CH_3OH, NaBr) positive ion: 889.22 $[M-Br-HBr]^+$.

Reaction of *cis-Cl,P,N*-[Fe(PN^H-Ph)$_2$Cl$_2$] (2a) in CD_3CN. Formation of *cis-N,P,N*-[Fe(PN^H-Ph)$_2$(CD$_3$CN)$_2$]$^{2+}$ (6). Upon dissolution of **2a** (20 mg) in ca 0.5 mL of CD_3CN a mixture of the dicationic complex *cis-N,P,N*-$[Fe(PN^H\text{-}Ph)_2(CD_3CN)_2]^{2+}$ (**6**) and a symmetrical isomer thereof (**7**) in a 2:1 molar ratio was afforded within 24h as monitored by ^{31}P{^{1}H} NMR spectroscopy. ^{31}P{^{1}H} NMR (δ, CD_3CN, 20°C): Isomer **6**: 114.6 (AB spin system, Δν = 533.2 Hz, J_{PP} = 54.8 Hz). Isomer **7**: 110.8 ppm. Crystals of **6** suitable for X-ray crystallography could be obtained by reacting **2a** in CH_3CN followed by slow diffusion of diethyl ether.

X-ray Structure Determination

Single crystals of the complexes **2b**, **5b**, and **6** suitable for X-ray diffraction were obtained by the solvent/antisolvent vapor diffusion method at room temperature using CH_2Cl_2/diethyl ether (**2b**), CH_3OH/diethyl ether (**5b**), and CH_3CN/diethyl ether (**6**). X-ray diffraction data were collected at *T* = 100 K on a Bruker Kappa APEX-2 CCD diffractometer using graphite-monochromated Mo-Kα radiation (λ = 0.71073 Å) and φ- and ω-scan frames covering complete spheres of the reciprocal space with θ_{max} = 30°. Corrections for absorption and λ/2 effects were applied using program SADABS.[27] After structure solution with program SHELXS97 refinement on F^2 was carried out with program SHELXL97[28] for **2b** and **6**. Non-hydrogen atoms were refined anisotropically. Hydrogen atoms were placed in calculated positions and thereafter treated as riding. Prior to final refinement of **6** a disordered CH_3CN solvent molecule (ca. 0.5 CH_3CN per Fe complex) was removed with procedure SQUEEZE of program PLATON.[29]

The structure of **5b** was solved with charge-flipping implemented in SUPERFLIP and refined with JANA2006.[30] Non-hydrogen atoms were refined anisotropically. Hydrogen atoms were placed in calculated positions and thereafter treated as riding except for N-bonded H atoms, which were refined freely. The N−H bond lengths were restrained to 0.870(1) Å. Due to disorder, the solvent molecules in **5b** could not be resolved and the electron density in the solvent voids corresponding to approximately 2.5 CH_3OH molecules per asymmetric unit was removed with procedure SQUEEZE of program PLATON.[25]

2b: $C_{36}H_{34}Cl_2FeN_4P_2$, M_r = 711.36, monoclinic, space group $P2_1/n$ (no. 14), a = 10.1491(3) Å, b = 12.8821(3) Å, c = 12.8714(3) Å, α = 90°, β = 103.291(2)°, γ = 90°, V = 1637.75(7) Å^3, Z = 2, μ = 0.755 mm^{-1}. Of 33383 reflections collected ($\theta \leq 30°$), 4749 were independent; R_{int} = 0.042; final R values: R_1 = 0.0356 ($I > 2\sigma(I)$), wR_2 = 0.0806 (all data).

5b: $C_{51}H_{45}Br_2FeN_6P_3$, M_r = 1050.5, orthorhombic, space group *Fdd2* (no. 43), a = 32.0762(14) Å, b = 35.738(2) Å, c = 35.738(2) Å, $\alpha = \beta = \gamma = 90°$, V = 22070(3) Å^3, Z = 16, μ = 1.845 mm^{-1}. Of 43656 reflections collected ($\theta \leq 30°$), 15186 were independent; R_{int} = 0.042; final R values: R_1 = 0.0373 ($I > 3\sigma(I)$), wR_2 = 0.0819 (all data). Flack parameter = -0.008(4).

6: $C_{38}H_{36}B_2F_8FeN_6P_2$, M_r = 868.14, triclinic, space group $P\bar{1}$ (no. 2), a = 10.7266(13) Å, b = 20.317(3) Å, c = 21.130(3) Å, α = 64.129(2)°, β = 83.943(2)°, γ = 89.942(2)°, V = 4115.1(9) Å^3, Z = 4, μ = 0.516 mm^{-1}. Of 67127 reflections collected ($\theta \leq 30°$), 23584 were independent; R_{int} = 0.048; final R values: R_1 = 0.0606 ($I > 2\sigma(I)$), wR_2 = 0.1649 (all data).

Computational Details

Calculations were performed using the GAUSSIAN 09 software package,[31] and the OPBE[32] functional without symmetry constraints. This functional was shown to perform well in mechanistic studies of spin forbidden reactions in related Fe systems.[33] It has to be noted however that while DFT is very successful at predicting geometries of both high-spin and low-spin complexes, obtaining the correct ground state represents a major challenge since GGA (generalized gradient approximation) functionals (e.g., OPBE, PBE) tend to favor the low-spin states, while the hybrid functionals (e.g., B3LYP, PBE0) artificially favor the high-spin states.[34,35] For example, the energy difference between the HS and LS states of *cis-Cl,P,N*-[Fe(PN^H-Ph)$_2$Cl$_2$] (**B**) is 4.5 kcal mol^{-1} when calculated with PBE[36] changing to 24.1 kcal mol^{-1} with PBE0[37] and to 18.4 kcal mol^{-1}, if B3LYP[38] is employed. With the exception of the PBE functional, data in all cases the HS state is more stable than LS state which is in agreement with the experimental data. The optimized geometries were obtained with the Stuttgart/Dresden ECP (SDD) basis set[39] to describe the electrons of the iron atom. For all other atoms a standard 6-31g** basis set was employed.[40] Frequency calculations were performed to confirm the nature of the stationary points yielding no imaginary frequency for the minima.

TD-DFT[41] calculations were performed to obtain the UV/Vis spectra of isomers **B** and **C** of complex **2a** (S=0 and S=2) using the formalism implemented on Gaussian 09. The OPBE functional was found to reproduce experimental spectra more reliably than others tested (CAM-B3LYP). The basis set was the same as for geometry optimization, with one added f polarization function.[42]

Mössbauer parameters (quadrupole splitting – ΔE_Q – and isomer shift – δ) were evaluated by performing single-point calculations at the B3LYP[34] level of theory with the ORCA software (Version 2.9.0),[20] on the optimized geometries. The value for ΔE_Q is directly given by the program, while the isomer shift was evaluated from the electron density at the Fe nucleus using the approach of Neese.[21] Fe was described by the triply polarized core properties basis set CP(PPP)[43] and the other atoms by the SV(P) basis set[44] with the inner s-functions uncontracted; the auxiliary basis set SV/J[45] was also used for these calculations (basis set b1). For Fe atom, an enhanced integration grid was used, and the overall integration accuracy was increased to 7.[21] Taking into account the results of a recent benchmark study[46] about the prediction of ^{57}Fe Mössbauer parameters by DFT, we also calculated both Mössbauer parameters, ΔE_Q and δ, with the Partridge-1 basis set[47] for Fe and cc-pVDZ basis set[48] for the other atoms (basis set b2).

Acknowledgements

Financial support by the Austrian Science Fund (FWF) (Project No. P24202-N17) is gratefully acknowledged. The ESI mass spectrometer was made available by Austrian Science Fund (FWF) (Project No. P15008-N03 to GA). The X-ray center of the Vienna University of Technology is acknowledged for financial support and for providing access to the single-crystal diffractometer. MJC, MDC and LPF acknowledge FCT (PEst-OE/QUI/UI0612/2013, PEst-OE/QUI/UI0536/2011, PEst-OE/FIS/UI0261/2011) for financial support and AG for a grant (SFRH/BPD/89722/2012). We also thank Christian Knoll, Johannes Ofner and Bernhard Lendl for the recording of Raman spectra. The support and sponsorship of COST action CM1205 “Catalytic Routines for Small Molecule Activation (CARISMA)” is also acknowledged.

Table 1. Estimated hyperfine parameters from the ^{57}Fe Mössbauer spectra of [Fe(PN^{H}-Ph)$_2$Cl$_2$] (**2a**) and [Fe(PN^{H}-Ph)$_2$Br$_2$] (**3a**) collected at different temperatures.

Compound	T (K)	δ (mm s^{-1})	ΔE_Q (mm.s^{-1})	Γ (mm s^{-1})	I (%)	Fe(II) site
[Fe(PN^{H}-Ph)$_2$Cl$_2$] (**2a**)	290	0.87(1)	3.11(1)	0.27(1)	100	HS
	195	0.92(1)	3.22(1)	0.28(2)	58.5	HS
		0.44(1)	1.00(1)	0.29(2)	41.5	LS
	170	0.96(1)	3.18(1)	0.26(2)	30.4	HS
		0.45(1)	0.99(1)	0.25(1)	69.6	LS
	78	1.10(3)	2.95(5)	0.63(9)	13.3	HS
		0.48(1)	0.98(1)	0.24(1)	86.7	LS
[Fe(PN^{H}-Ph)$_2$Br$_2$] (**3a**)	290	0.87(1)	3.09(1)	0.26(1)	100	HS
	215	0.91(1)	3.25(1)	0.30(1)	44.8	HS
		0.44(1)	1.04(1)	0.31(1)	55.2	LS
	185	0.92(1)	3.23(3)	0.39(4)	20.9	HS
		0.46(1)	1.04(1)	0.26(1)	79.1	LS
	78	1.08(2)	3.32(4)	0.41(7)	8.5	HS
		0.48(1)	1.03(1)	0.25(1)	91.5	LS

δ – isomer shift; ΔE_Q – quadrupole splitting; Γ – FWHM line width;
I – relative area with uncertainties < 2%.

Table 2. Estimated hyperfine parameters from the ^{57}Fe Mössbauer spectra of [Fe(PN^{Me}-Ph)$_2$Cl$_2$] (**2b**) and [Fe(PN^{Me}-Ph)$_2$Br$_2$] (**3b**) collected at 290 K.

Compound	δ (mm s^{-1})	ΔE_Q (mm s^{-1})	Γ (mm.s^{-1})	Fe(II) site
[Fe(PN^{Me}-Ph)$_2$Cl$_2$] (**2b**)	0.85(1)	3.04(1)	0.26(1)	HS [a]
[Fe(PN^{Me}-Ph)$_2$Br$_2$] (**3b**)	0.88(1)	3.14(1)	0.27(1)	HS

δ – isomer shift; ΔE_Q – quadrupole splitting; Γ – FWHM line width.

[a] A small impurity due to oxidation during Mössbauer sample preparation is also present.

Table 3. Elemental compositions of the neutral compounds **2**, **3**, **5** and calculated m/z values of $[M–X]^+$ (compounds **2** and **3**), $[M–X–HX]^+$ (compounds **2**, **3**, **5**) and [M–X–HX–**1a**/**b**) ions (compounds **2**, **3**, **5**; X = Cl, Br).

Compound	Elemental composition/ Molecular weight [a]	Elemental composition	Elemental composition
2a	$C_{34}H_{30}Cl_2Fe_1N_4P_2$ 682.07	$C_{34}H_{30}Cl_1Fe_1N_4P_2$ $[M–Cl]^+$ = 647.10	$C_{34}H_{29}Fe_1N_4P_2$ $[M–Cl–HCl]^+$ = 611.12 $C_{17}H_{15}Cl_1Fe_1N_1P_1$ $[M–Cl–$**1a**$]^+$ = 369.00
2b	$C_{36}H_{34}Cl_2Fe_1N_4P_2$ 710.10	$C_{36}H_{34}Cl_1Fe_1N_4P_2$ $[M–Cl]^+$ = 675.13	$C_{18}H_{17}Cl_1Fe_1N_1P_1$ $[M–Cl–$**1b**$]^+$ = 383.02
3a	$C_{34}H_{30}Br_2Fe_1N_4P_2$ 769.97	$C_{34}H_{30}Br_1Fe_1N_4P_2$ $[M–Br]^+$ = 691.05	$C_{34}H_{29}Fe_1N_4P_2$ $[M–Br–HBr]^+$ = 611.12 $C_{17}H_{15}Br_1Fe_1N_1P_1$ $[M–Br–$**1a**$]^+$ = 412.95
3b	$C_{36}H_{34}Br_2Fe_1N_4P_2$ 798.00	$C_{36}H_{34}Br_1Fe_1N_4P_2$ $[M–Br]^+$ = 719.08	$C_{18}H_{17}Br_1Fe_1N_1P_1$ $[M–Br–$**1b**$]^+$ = 426.97
5a	$C_{51}H_{45}Cl_2Fe_1N_6P_3$ 960.16	$C_{51}H_{44}Fe_1N_6P_3$ $[M–Cl–HCl]^+$ = 889.22	$C_{34}H_{29}Fe_1N_4P_2$ $[M–Cl–HCl–$**1a**$]^+$ = 611.12
5b	$C_{51}H_{45}Br_2Fe_1N_6P_3$ 1048.06	$C_{51}H_{44}Fe_1N_6P_3$ $[M–Br–HBr]^+$ = 889.22	$C_{34}H_{29}Fe_1N_4P_2$ $[M–Br–HBr–$**1a**$]^+$ = 611.12

[a] Mass calculations are based on the lowest mass chlorine (^{35}Cl) and bromine isotope (^{79}Br), respectively, and the most abundant iron isotope (^{56}Fe).

Table 4. Mean Fe-P, Fe-N_{py}, and Fe-Cl bond lengths (Å) for complexes **2b**, [*trans*-$Fe(PP)_2Cl_2$] (PP = *cis*-1,2-bis(diphenylphosphino)ethylene),[17] $\mathbf{A}^{HS}$, $\mathbf{A}^{LS}$, $\mathbf{B}^{HS}$, $\mathbf{B}^{LS}$, **5**, and **6**.

complexes	spin state	Fe-P	Fe-N	Fe-Cl
2b	HS	2.605	2.191	2.364
$[Fe(PP)_2Cl_2]$	HS	2.584		2.363
$[Fe(PP)_2Cl_2]$	LS	2.301		2.329
$\mathbf{A}^{HS}$	HS	2.687	2.325	2.332
$\mathbf{A}^{LS}$	LS	2.253	2.012	2.313
$\mathbf{B}^{HS}$	HS	2.612	2.397	2.350
$\mathbf{B}^{LS}$	LS	2.159	2.033	2.337
5	LS	2.245	2.049	
6	LS	2.215	2.020	

References

1 (a) A. Bader and E. Lindner, *Coord. Chem. Rev.* 1991, **108**, 27 and references therein; (b) M. Bassetti, *Eur. J. Inorg. Chem.* 2006, 4473; (c) G. Helmchen and A. Pfaltz, *Acc. Chem. Res.* 2000, **33**, 336; (d) H. A. McManus and P. Guiry, *Chem. Rev.* 2004, **104**, 4151; (e) P. Braunstein, *Chem. Rev.* 2006, **106**, 134; (f) V. V. Grushin, *Chem. Rev.* 2004, **104**, 1629. (g) T. Q. Ly and J. D. Woollins, *Coord. Chem. Rev.* 1998, **176**, 451.

2 J. Ansell and M. Wills, *Chem. Soc. Rev.* 2002, **31**, 259.

3 (a) C. Holzhacker, C. M. Standfest-Hauser, M. Puchberger, K. Mereiter, L. F. Veiros, M. J. Calhorda, M. D. Carvalho, L. P. Ferreira, M. Godinho, F. Hartl and K. A. Kirchner, *Organometallics* 2011, **30**, 6587; (b) B. Bichler, M. Puchberger, L. F. Veiros, Ö. Öztopcu, K. Mereiter, K. A. Kirchner, *Organometallics* 2011, **30**, 5928; (c) C. M. Standfest-Hauser, G. Dazinger, J. Wiedermann, K. Mereiter and K. Kirchner, *Eur. J. Inorg. Chem.* 2009, 4085; (d) W. Lackner-Warton, S. Tanaka and C. M. Standfest-Hauser, Ö. Öztopcu, J.-C. Hsieh, K. Mereiter and K. Kirchner, *Polyhedron* 2010, **29**, 3097; (e) D. Benito-Garagorri, K. Mereiter and K. Kirchner, *Collect. Czech. Chem. Commun.* 2007, **72**, 527.

4 W.-J. Zhao, S.-J. Zhang, Y. Deng, Z.-Z. Zhang, Y.-F. Ma, W.-P. Huang and H.-G. Wang, *Jiegou Huaxue* 1996, **15**, 44.

5 W. Seidel and H. Schöler, *Z. Chem.* 1967, **11**, 431.

6 W. Ainscough and L. K. Peterson, *Inorg. Chem.* 1970, **9**, 2699.

7 H. Brunner and H. Weber, *Chem. Ber.* 1985, **118**, 3380.

8 (a) W. Schirmer, U. Flörke and H. J. Haupt, *Z. Anorg. Allg. Chem.* 1987, **545**, 83; (b) W. Schirmer, U. Flörke and H. J. Haupt, *Z. Anorg. Allg. Chem.* 1989, **574**, 239.

9 S. M.Aucott, A. M. Z. Slawin and J. D. Woollins, *Phosphorus, Sulfur, and Silicon* 1997, **124**-**125**, 473.

10 (a) S. M.Aucott, A. M. Z. Slawin and J. D. Woollins, *J. Chem. Soc. Dalton Trans.* 2000, 2559; (b) M. L. Clarke, A. M. Z. Slawin, M. V. Wheatley and J. D. Woollins, *J. Chem. Soc. Dalton Trans.* 2001, 3421; (c) A. M. Z. Slawin, J. Wheatley, M. V. Wheatley and J. D. Woollins, *Polyhedron* 2003, **22**, 1397.

11 G. Sanchez, J. Garcia, D. Meseguer, J. L. Serrano, L. Garcia, J. Perez and G. Lopez, *Inorg. Chim. Acta* 2004, **357**, 4568.

12 (a) E. Smolensky, M. Kapon, J. D. Woollins and M. S. Eisen, *Organometallics* 2005, **24**, 3255; (b) E. Smolensky, M. Kapon and M. S. Eisen, *Organometallics* 2007, **26**, 4510.

13 S. M. Nabavizadeh, E. S. Tabei, F. N. Hosseini, N. Keshavarz, S. Jamali and M. Rashidi, *New J. Chem.* 2010, **34**, 495.

14 B. Blank, G. Glatz and R. Kempe, Chem. Asian J. 2009, **4**, 321.

15 (a) I. Hyder, M. Jimenez-Tenorio, M. C. Puerta and P. Valerga, *Organometallics* 2011, **30**, 726; (b) I. Macias-Arce, M. C. Puerta and P. Valerga, *Eur. J. Inorg. Chem.* 2010, 1767.

16 (a) W. Seidel and I. Bürger, Z. Chem. 1973, **137**, 260; (b) W. Seidel and H. Schöler, Z. Chem. 1967, **7**, 431.

17 (a) F. Cecconi, M. Di Vaira, S. Midollini, A. Orlandini, L. Sacconi, *Inorg. Chem.* 1981, **20**, 3423; (b) M. Di Vaira, S. Midollini, L. Sacconi, *Inorg. Chem.* 1981, **20**, 3430. (c) C.-C. Wu, J. Jung, P. K. Gantzel, P. Gütlich, and D. N. Hendrickson, *Inorg. Chem.* 1997, **36**, 5339.

18 P. Gütlich, A. B. Gaspar and Y. Garcia, *Beilstein J. Org. Chem.* 2013, **9***,* 342.

19 Y. Garcia, V. Ksenofontov and P. Gütlich, *Hyperfine Interact.* 2002, **139/140,** 543.

20 F. Neese, ORCA – an ab initio, Density Functional and Semi-empirical Program Package, Version 2.9.0, January 2012, Max-Planck-Institut für Bioanorganische Chemie, Mülheim/Ruhr, 2012.

21 (a) F. Neese, *Inorg. Chim.Acta* 2002, **337**, 181; (b) F. Neese, *Coord. Chem. Rev.* 2009, **252**, 526.

22 D. Benito-Garagorri, L. G. Alves, M. Puchberger, K. Mereiter, L. F. Veiros, M. J. Calhorda, M. D. Carvalho, L. P. Ferreira, M. Godinho and K. Kirchner, *Organometallics,* 2009, **28**, 6902.

23 D. D. Perrin, W. L. F. Armarego, *Purification of Laboratory Chemicals*, 3rd ed.; Pergamon: New York, 1988.

24 (a) W. J. Knebel and R. J. Angelici, *Inorg. Chim. Acta* 1973, **7**, 713; (b) W. J. Knebel and R. J. Angelici, *Inorg. Chem.* 1974, **13**, 632; (c) E. W. Ainscough, A. M. Brodie and S. T. Wong, *J. Chem. Soc., Dalton Trans.* 1977, 915.

25 S. R. M. M. de Aguiar, B. Stöger, E. Pittenauer, G. Allmaier, M. Puchberger, L. F. Veiros and K. Kirchner, *J. Organomet. Chem.* 2014, in press (10.1016/j.jorganchem.2013.12.018).

26 (a) C. Maurer, E. Pittenauer, V. A. Du, G. Allmaier, U. Schubert, *Dalton Trans.* 2012, **41**, 2346. (b) C. Maurer, E. Pittenauer, M. Puchberger, G. Allmaier, U. Schubert, *ChemPlusChem* 2013, **78**, 343.

27 Bruker programs: *APEX2*, version 2009.9–0; *SAINT*, version 7.68 A; *SADABS*, version 2008/1; *SHELXTL*, version 2008/4, Bruker AXS Inc., Madison, WI, 2009.

28 G. M. Sheldrick, *Acta Cryst.* 2008, **A64**, 112.

29 A. L. Spek,. Acta Cryst. 2009, **D65**, 148.

30 V. Petříček, M. Dušek and L. Palatinus, 2006. JANA2006. Institute of Physics, Praha, Czech Republic.

31 Gaussian 09, Revision A.02, M. J. Frisch, G. W. Trucks, H. B. Schlegel, G. E. Scuseria, M. A. Robb, J. R. Cheeseman, G. Scalmani, V. Barone, B. Mennucci, G. A. Petersson, H. Nakatsuji, M. Caricato, X. Li, H. P. Hratchian, A. F. Izmaylov, J. Bloino, G. Zheng, J. L. Sonnenberg, M. Hada, M. Ehara, K. Toyota, R. Fukuda, J. Hasegawa, M. Ishida, T. Nakajima, Y. Honda, O. Kitao, H. Nakai, T. Vreven, J. A. Montgomery, Jr., J. E. Peralta, F. Ogliaro, M. Bearpark, J. J. Heyd, E. Brothers, K. N. Kudin, V. N. Staroverov, R. Kobayashi, J. Normand, K. Raghavachari, A. Rendell, J. C. Burant, S. S. Iyengar, J. Tomasi, M. Cossi, N. Rega, J. M. Millam, M. Klene, J. E. Knox, J. B. Cross, V. Bakken, C. Adamo, J. Jaramillo, R. Gomperts, R. E. Stratmann, O. Yazyev, A. J. Austin, R. Cammi, C. Pomelli, J. W. Ochterski, R. L. Martin, K. Morokuma, V. G. Zakrzewski, G. A. Voth, P. Salvador, J. J. Dannenberg, S. Dapprich, A. D. Daniels, Ö. Farkas, J. B. Foresman, J. V. Ortiz, J. Cioslowski, and D. J. Fox, Gaussian, Inc., Wallingford CT, 2009.

32 (a) N. C. Handy and A. Cohen, *J. Mol. Phys.* 2001, **99**, 403; (b) W.-M. Hoe, A. Cohen and N. C. Handy, *Chem. Phys. Lett.*, 2001, **341**, 319.

33 (a) M. Swart, A. R. Groenhof, A. W. Ehlers and K. Lammertsma, *J. Phys. Chem A* 2004, **108**, 5479; (b) M. Swart, A. W. Ehlers and K. Lammertsma, *Mol. Phys.* 2004, **102**, 2467; (c) M. Swart, *Inorg. Chim. Acta* 2007, **360**, 179; (d) M. Swart, *J. Phys. Chem A* 2008, **112**, 6384; (e) M. Swart, *J. Chem. Theory Comput.* 2008, **4**, 2057; (e) J. Conradie and A. Ghosh, *J. Chem. Theory Comput.* 2007, **3,** 689.

34 D. N. Bowman and E. Jakubikova, *Inorg. Chem.* 2012, **51**, 6011.

35 S. Ye, F. Neese, *Inorg. Chem.* 2010*,* **49***,* 772.

36 (a) J. P. Perdew, K. Burke and M. Ernzerhof, *Phys. Rev. Lett.* 1996, **77**, 3865; (b) J. P. Perdew, K. Burke and M. Ernzerhof, *Phys. Rev. Lett.* 1997, *78*, 1396.

37 C. Adamo and V. Barone, *J. Chem. Phys.*, 1999, **110,** 6158.

38 (a) A. D. Becke, *J. Chem. Phys.* 1993, **98**, 5648; (b) B. Miehlich, A. Savin, H. Stoll and H. Preuss, *Chem. Phys. Lett* 1989, **157**, 200; (c) C. Lee, W. Yang and G. Parr, *Phys. Rev. B* 1988, **37**, 785.

39 (a) U. Haeusermann, M. Dolg, H. Stoll, H. Preuss, *Mol. Phys.* 1993, **78**, 1211; (b) W. Kuechle, M. Dolg, H. Stoll and H. Preuss, *J. Chem. Phys.* 1994, **100**, 7535; (c) T. Leininger, A. Nicklass, H. Stoll, M. Dolg and P. Schwerdtfeger, *J. Chem. Phys.* 1996, **105**, 1052.

40 (a) A. D. McLean and G. S. Chandler, *J. Chem. Phys.* 1980, **72**, 5639; (b) R. Krishnan, J. S. Binkley, R. Seeger and J. A. Pople, *J. Chem. Phys.* 1980, **72**, 650; (c) P. J. Hay, *J. Chem. Phys.* 1977, **66**, 4377; (d) K. Raghavachari and G. W. Trucks, *J. Chem. Phys.* 1989, **91**, 1062; (e) R. C. Binning and L. A. Curtiss, *J. Comput. Chem.* 1995, *10*3, 6104; (f) M. P. McGrath and L. Radom, *J. Chem. Phys.* 1991, **94**, 511.

41 (a) R. E. Stratmann, G. E. Scuseria and M. J. Frisch, *J. Chem. Phys.* 1998, **109**, 8218. (b) R. Bauernschmitt and R.Ahlrichs, *Chem. Phys. Lett.* 1996, **256**, 454. (c) M. E. Casida, C. Jamorski, K. C. Casida and D. R. Salahub, *J. Chem. Phys.* 1998, **108**, 4439.

42 V. Rassolov, J. A. Pople, M. Ratner and T. L. Windus, *J. Chem. Phys*. 1998, **109**, 1223.

43 (a) The ORCA basis set 'CoreProp' was used. This basis is based on the TurboMole DZ bases developed by Ahlrichs and coworkers and obtained brom the basis set library under ftp.chemie.uni-karlsruhe.de/pub/basen. (b) The Ahlrichs (2d2fg,3p2df) polarization functions were obtained from the Turbomole basis set library under ftp.chemie.uni-karlsruhe.de/pub/basen Sc-Zn: 2p functions from J. Wachters *Chem. Phys*. 1970, **52**, 1033 plus one f-function from the TurboMole library.

44 A. Schäfer, H. Horn and R. Ahlrichs, *J. Chem. Phys.* 1992, **97**, 2571.

45 The Ahlrichs auxiliary basis sets were obtained from the TurboMole basis set library under ftp.chemie.uni-karlsruhe.de/pub/jbasen H-Ba; Hf-At: (a) K. Eichkorn, O. Treutler, H. Ohm, M. Haser and R. Ahlrichs, *Chem. Phys. Lett.* 1995, **240**, 283; (b) K. Eichkorn, F. Weigend, O. Treutler and R. Ahlrichs, *Theor. Chem. Acc.* 1997, **97**, 119.

46 A. D. Bochevarov, R. A. Friesner and S. J. Lippard, *J. Chem. Theory Comput.* 2010, **6**, 3735.

47 H. Partridge, *J. Chem. Phys.* 1989, **90**, 1043.

48 (a) T. H. Dunning, Jr., *J. Chem. Phys.* 1989, **90**, 1007; (b) D. E. Woon and T. H. Dunning, Jr., *J. Chem. Phys.* 1993, **98**, 1358.

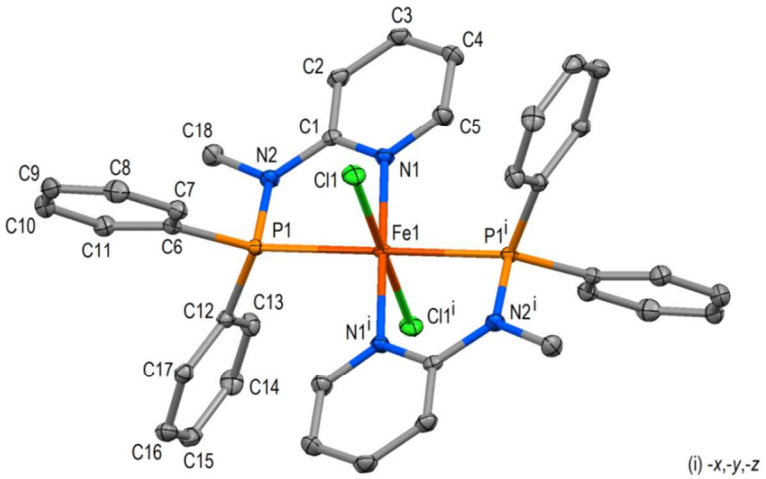

Figure 1. Structural view of *trans-Cl,P,N*-[Fe(PN^{Me}-Ph)$_2$Cl$_2$] (**2b**) showing 50% thermal ellipsoids (H atoms omitted for clarity). The complex is centrosymmetric. Selected bond lengths (Å) and bond angles (°): Fe1−N1 2.1910(13), Fe1−P1 2.6046(4), Fe1−Cl1 2.3637(4), P1−N2 1.7195(14), N2−C18 1.469(2), N2−C1 1.394(2), N1−Fe1−P1 75.80(4), N1−Fe1−P1^i 104.20(4), N1−Fe1−Cl1 88.67(4), N1−Fe1−Cl1^i 91.33(4), P1−Fe1−Cl1 94.83(1), P1−F1−Cl1^i 85.17(1), Cl1−Fe1−Cl1^i = P1−Fe−P1^i = N1−Fe1−N1^i = 180.00.

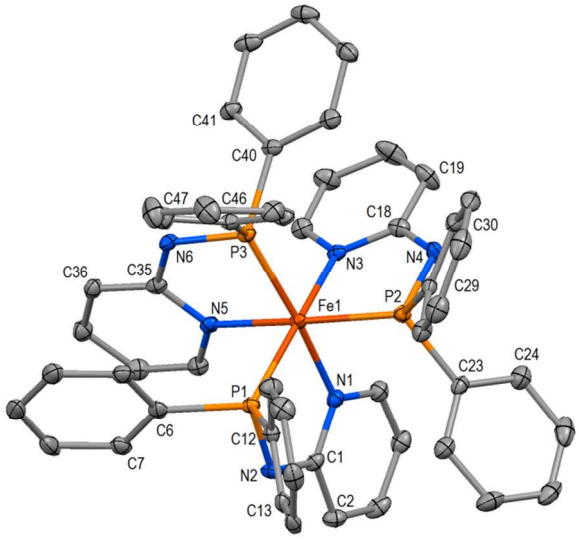

Figure 2. Structural view of *cis-P,N*-[Fe(PN^H-Ph)$_3$]Br$_2$ (**5b**) showing 50% thermal ellipsoids (H atoms and bromide anions omitted for clarity). Selected bond lengths (Å) and bond angles (°): Fe1−N1 2.042(2), Fe1−N3 2.048(2), Fe1−N5 2.058(2), Fe1−P1 2.2396(7), Fe1−P2 2.2546(8), Fe1−P3 2.2401(7), P1−N2 1.697(2), P2−N4 1.684(2), P3−N6 1.679(2), N1−Fe1−P1 83.44(6), N3−Fe1−P2 83.16(6), N5−Fe1−P3 82.72(6), N1−Fe1−N3 90.43(8), N1−Fe1−N5 89.33(8), N3−Fe1−N5 90.01(8), P1−Fe1−P2 102.40(3), P1−Fe1−P3 98.54(3), P2−Fe1−P3 100.63(3), N1−Fe1−P3 171.53(7), N3−Fe1−P1 171.43(6), N5−Fe1−P2 172.18(6).

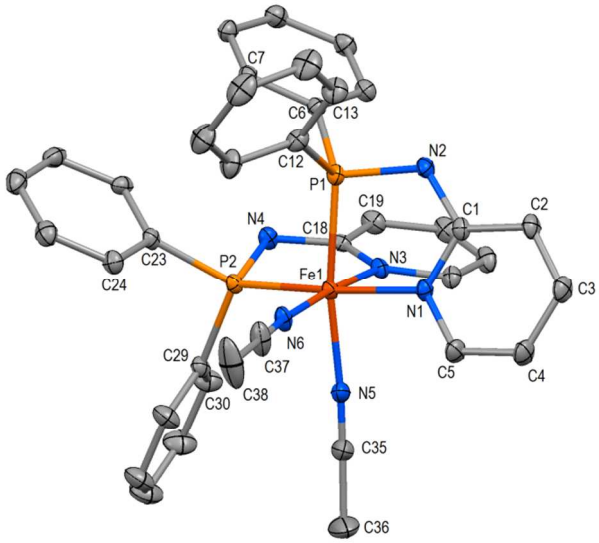

Figure 3. Structural view of *cis-P,N,N*-[Fe(PN^{H}-Ph)$_2$(CH$_3$CN)$_2$](BF$_4$)$_2$ (**6**) showing 50% thermal ellipsoids (H atoms, BF_4^- anions, and second independent Fe complex omitted for clarity). Selected bond lengths (Å) and bond angles (°): Fe1−N1 2.034(2), Fe1−N3 2.006(2), Fe1−N5 1.966(3), Fe1−N6 1.918(3), Fe1−P1 2.2241(9), Fe1−P2 2.2056(8), P1−N2 1.693(3), P2−N4 1.680(3), N2−C1 1.379(4), N4−C18 1.383(4), N1−Fe1−P1 81.03(8), N3−Fe1−P2 82.03(7), N1−Fe1−N3 91.18(10), N1−Fe1−N5 91.28(11), N1−Fe1−N6 88.61(10), N5−Fe1−N6 88.03(12), P1−Fe1−P2 96.86(3), N1−Fe1−P2 172.97(8), N3−Fe1−N6 175.89(12), N5−Fe1−P1 171.28(8), P1−N2−C1 116.8(2), P2−N4−C18 116.5(2).

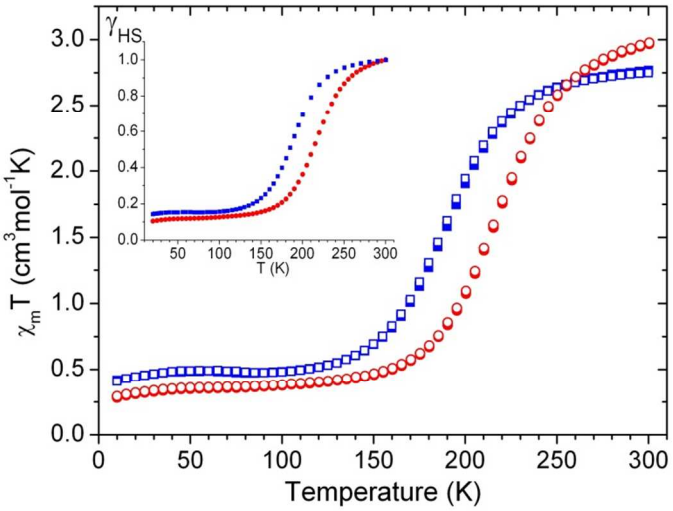

Figure 4. Temperature dependence of $\chi_m T$ for [Fe(PN^{H}-Ph)$_2$Cl$_2$] (**2a**) (blue squares) and [Fe(PN^{H}-Ph)$_2$Br$_2$] (**3a**) (red circles) upon cooling (solid symbols) and warming (open symbols). The inset shows the temperature variation of the HS Fe(II) mole fraction for both compounds, assuming that at 300 K there is only HS.

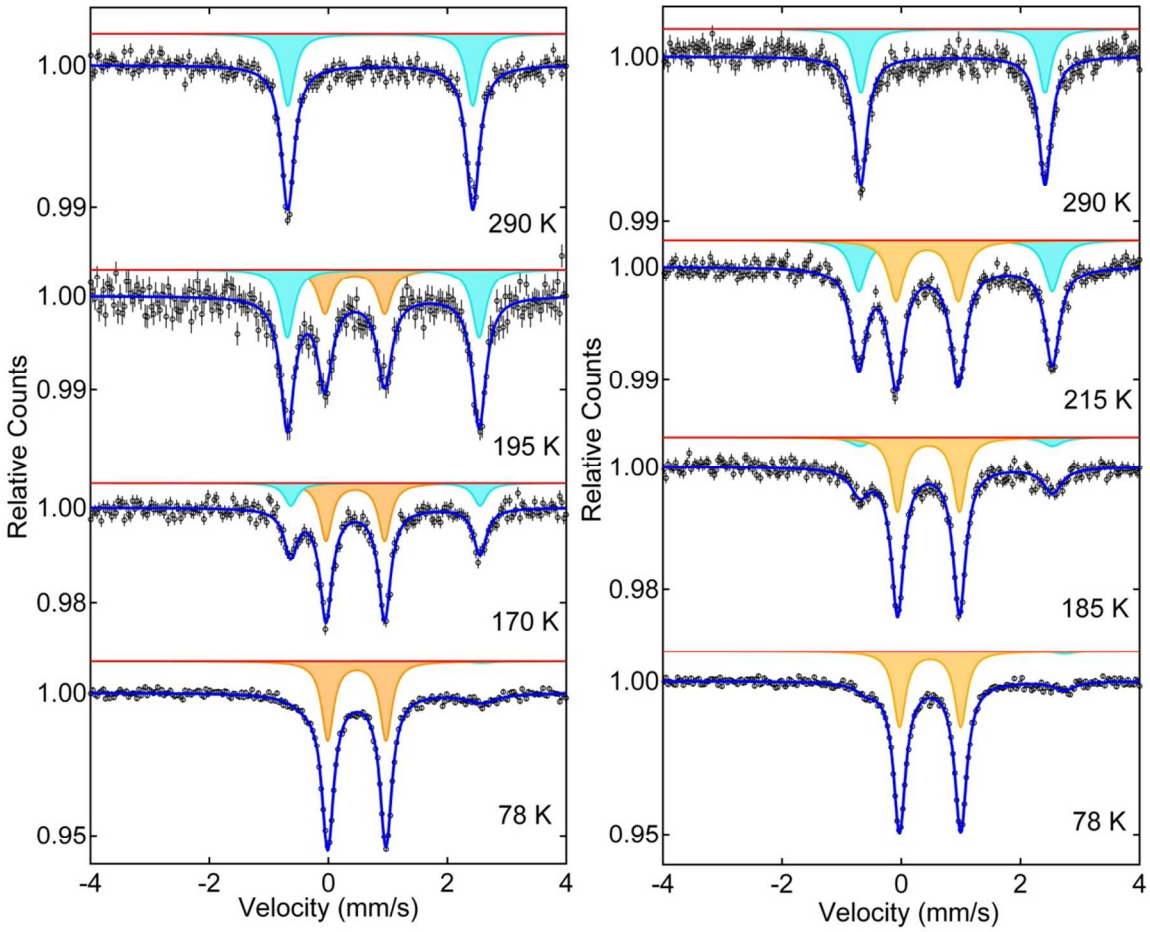

Figure 5. Temperature dependence of ^{57}Fe Mössbauer spectra of [Fe(PN^{H}-Ph)$_2$Cl$_2$] (**2a**) (left) and [Fe(PN^{H}-Ph)$_2$Br$_2$] (**3a**) (right).

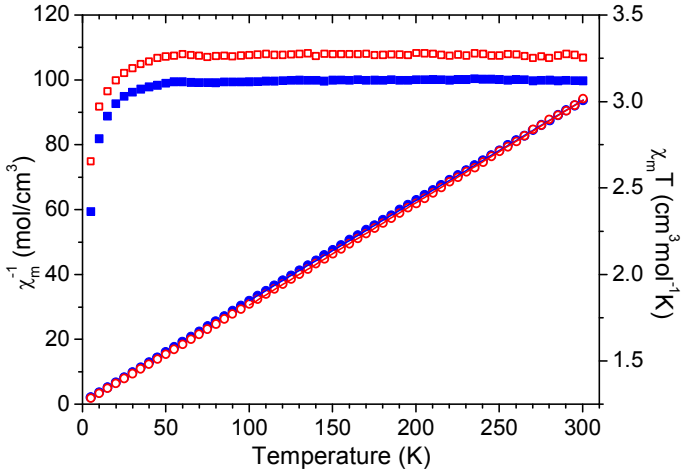

Figure 6. Temperature dependence of the inverse molar susceptibility (circles) and of χ_mT (squares) for [Fe(PN^{Me}-Ph)$_2$Cl$_2$] (**2b**) (solid symbols) and [Fe(PN^{Me}-Ph)$_2$Br$_2$] (**3b**) (open symbols). The straight lines correspond to Curie law fittings to the experimental data.

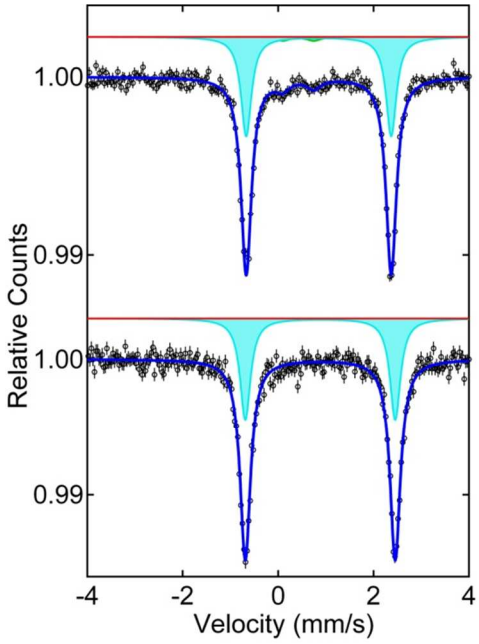

Figure 7. ^{57}Fe Mössbauer spectra of [Fe(PN^{Me}-Ph)$_2$Cl$_2$] (**2b**) (top) and [Fe(PN^{Me}-Ph)$_2$Br$_2$] (**3b**) (bottom) collected at 290 K.

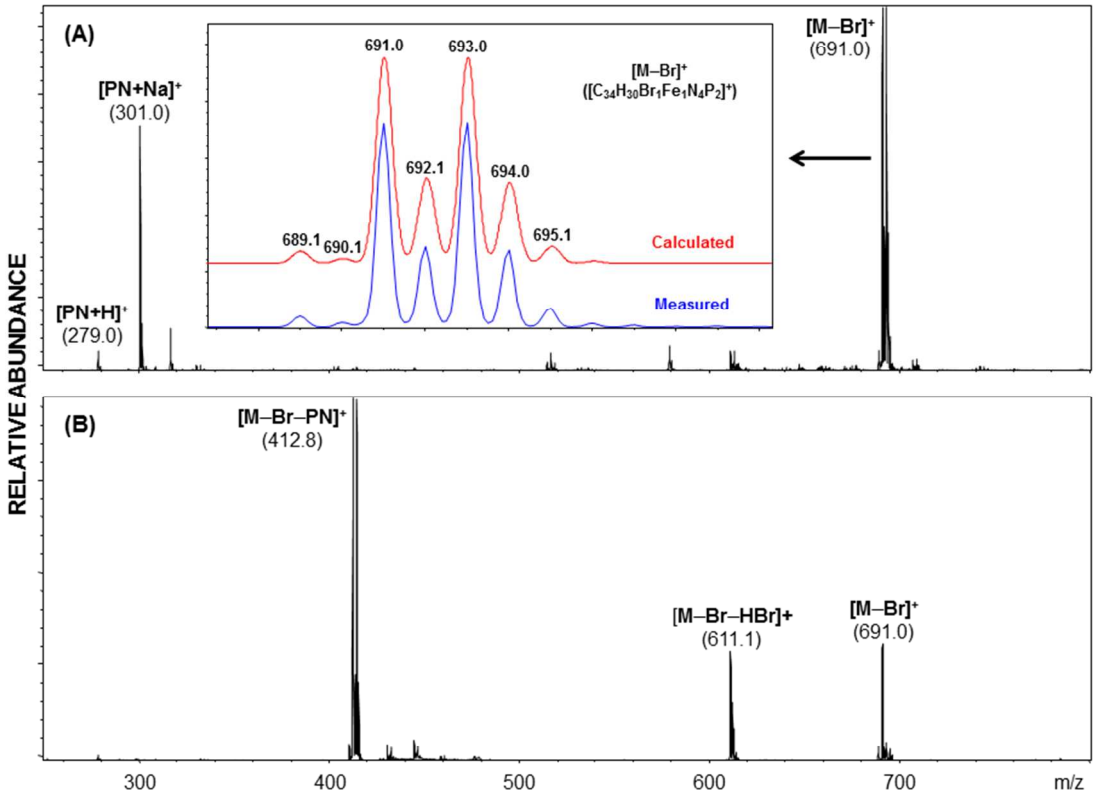

Figure 8. Positive-ion ESI full scan mass spectrum of [Fe(PN^{H}-Ph)$_2$Br$_2$] (**3a**) (**A**) and corresponding MS/MS (low energy CID)-spectrum of *in-source*-generated [M-Br]$^+$ precursor ion (m/z 691.0) (**B**). Inset shows the calculated and measured isotopic pattern of [M-Br]$^+$. In both spectra only signals containing the Fe-isotope of highest abundance (^{56}Fe) are annotated.

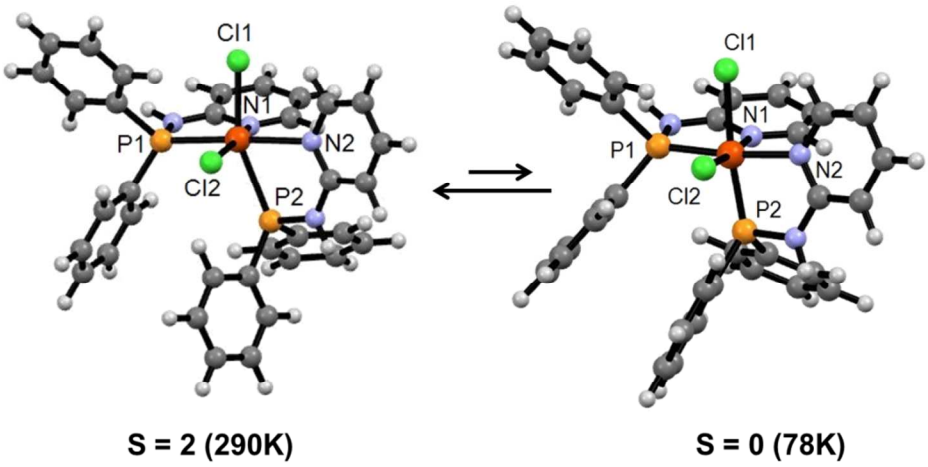

Figure 9. Optimized geometries of *cis*-*Cl,P,N*-[Fe(PN^{H}-Ph)$_2$Cl$_2$] (**B**) in spin states S = 2 (**B**^{HS}, left) and S = 0 (**B**^{LS}, right). Selected bond lengths (Å) for **B**^{HS}: Fe-P1 2.529, Fe-P2 2.695, Fe-N1 2.388, Fe-N2 2.406, Fe-Cl1 2.379, Fe-Cl2 2.320. **B**^{LS}: Fe-P1 2.151, Fe-P2 2.167, Fe-N1 1.967, Fe-N2 2.098, Fe-Cl1 2.351, Fe-Cl2 2.322.